Letter

Negative-travel-time quantum orbits in strong-field ionization by an elliptically polarized laser field

D. B. Milošević [1,2,3,*] and W. Becker [3]

[1]*Faculty of Science, University of Sarajevo, Zmaja od Bosne 35, 71000 Sarajevo, Bosnia and Herzegovina*
[2]*Academy of Sciences and Arts of Bosnia and Herzegovina, Bistrik 7, 71000 Sarajevo, Bosnia and Herzegovina*
[3]*Max-Born-Institut, Max-Born-Strasse 2a, 12489 Berlin, Germany*

(Received 17 December 2021; accepted 14 March 2022; published 24 March 2022)

A long-standing problem in quantum-orbit theory has been exactly which solutions of the saddle-point equations to include in the decomposition of the ionization or harmonic-generation amplitude. Up to now, solutions corresponding to a negative travel time have always been discarded. For the case of an elliptically polarized driving laser field, we show that certain solutions with a negative travel time are relevant and have to be included, in addition to the customary orbits with positive travel times, in order to achieve good agreement with the result of a numerical evaluation. In fact, these solutions are responsible for a pronounced qualitative effect in the high-order above-threshold ionization amplitude: a feature with the shape of a coffee bean split along the direction of the major polarization axis, which dominates the velocity map especially for long wavelength. We also discuss the electron trajectories in complex space and time that correspond to these orbits.

DOI: 10.1103/PhysRevA.105.L031103

Quantum orbits have become a powerful tool for the analysis of strong-field processes such as high-order harmonic generation (HHG) and (high-order) above-threshold ionization [(H)ATI]. Formally, they are derived by a steepest-descent evaluation of the corresponding emission or ionization amplitudes, which yields complex times of ionization, recombination, or rescattering, respectively, for the responsible electron and for the trajectories in between these times [1,2]; for reviews, see [3,4]. Quantum orbits are complex due to the electron's emergence in the continuum via tunneling. Intuitively, the real parts of the orbits depict the electronic trajectories underlying the process, and they largely agree with those of the simple-man model [3,5,6]. A stationary-phase evaluation of an expansion of Feynman's path integral in terms of the binding potential leads to the same quantum orbits [7,8].

Quantum-orbit theory has been instrumental for the analysis of the plateaus of HHG and HATI by identifying the responsible orbits and, via their phases, determining their interference [9]. Normally, very few orbits contribute and their interference dominates the spectrum (recall the short and the long orbit of HHG, whose manipulation is crucial for the design of high-harmonic sources [10,11]), but occasionally the constructive interference of a large number of orbits may generate strong enhancements of certain spectral regions [12,13]. For few-cycle pulses, quantum-orbit analysis allows one to extract the value of the carrier-envelope phase from the HATI spectrum [14,15]. At the lower end of the plateaus and for ATI in the region of direct electrons, more and more orbits are required for a satisfactory description of the data [16]. Yet, most of the conspicuous features observed for low energies, such as the low-energy structures (LES) [17,18] on the field-polarization axis and various structures off this axis (V structure, fork, etc.) [19–22], can be traced back to certain quantum orbits. However, the approximation of the spectra by quantum-orbit contributions has not been as good as it is for higher electron energies. Moreover, finding all pertinent quantum orbits is not an easy task, especially for fields other than the standard linearly polarized field.

In this Letter, we consider a monochromatic elliptically polarized field and report on certain quantum orbits that so far have been largely overlooked or ignored. These are orbits with their travel times (rescattering minus ionization times) so short that they are mostly or entirely confined to the inside of the tunneling barrier [23]. The imaginary parts of the travel times may be large and their real parts may even be negative. The large imaginary parts impede a straightforward intuitive physical interpretation. The negative travel time is not as counterintuitive as it may appear as long as the orbit is restricted to the inside of the tunneling barrier as is the case. In fact, the electrons are temporarily "captured" inside the potential barrier as this will follow from the complex-time quantum-orbit formalism which we will introduce. We will see that inclusion of these orbits dramatically improves the quality of the quantum-orbit approximation. Equally importantly, it yields qualitatively different structures in the velocity map of the rescattered electrons for elliptically polarized fields. In the present case, this is a structure in the angle-resolved momentum distribution of the rescattered electrons with a shape reminiscent of a coffee bean with the two halves oriented along the major axis of the polarization ellipse.

These orbits have also been discussed and utilized in [24,25] for linear polarization where negative travel times do not occur. The emphasis was on an estimate of the tunneling time delay; hence the orbits were not systematically

*Corresponding author: milo@bih.net.ba

embedded into the framework of quantum-orbit theory. The latter is able to reproduce solutions of the time-dependent Schrödinger equation with remarkably high precision, at least for short-range binding potentials, but only if all relevant orbits are taken into account. The orbits to be discussed here are especially important in the difficult region of comparatively low electron energy where the Coulomb potential is very important [26,27]. It should be mentioned that quantum orbits account for the Coulomb potential only via the initial-state wave function and in the act of rescattering. This limitation has been in the focus of intense recent research [28–31]; for a review, see [32]. However, the existence of the solutions, discussed in this Letter, is not affected; they will only be modified by the Coulomb potential.

In earlier works for a linearly polarized monochromatic field, we introduced a classification of the pertinent orbits as backscattering orbits characterized by the multi-index (α, β, m) [33] and forward-scattering orbits characterized by (ν, μ) [34]. For more complex fields, this classification has to be extended [35]. In the present contribution, we consider HATI by an elliptically polarized monochromatic field. Here, we trace the aforementioned coffee-bean structure to an orbit to be denoted by $(1, 1, 0)^*$, which is responsible for this effect, as will be explained below. This structure is particularly pronounced for longer wavelengths.

We illustrate the effect by the detachment of an electron off an F^- ion by an elliptically polarized field with the intensity 1.3×10^{13} W/cm^2 at mid-IR wavelengths up to 5500 nm. For details of the modeling, see [36].

The differential ionization rate for detection of an electron with the momentum $\mathbf{p}$ and with absorption of n photons from the laser field is given by [4,35] $\sum_{M=-\ell}^{\ell} w_{\mathbf{p}E_i\ell M}(n)$, where $E_i = -I_p$ is the binding energy and we average over the magnetic quantum number M because the ground state of the F^- ion has the orbital quantum number $\ell = 1$. Within our improved strong-field approximation the rate is given by $w_{\mathbf{p}E_i\ell M}(n) \approx 2\pi p |T^{\rm dir}_{\mathbf{p}E_i\ell M}(n) + T^{\rm res}_{\mathbf{p}E_i\ell M}(n)|^2$, with the energy-conservation condition $n\omega = E_{\mathbf{p}} - E_i + U_p$, where $U_p = \int_0^T dt\, \mathbf{A}^2(t)/(2T)$ is the ponderomotive energy, $T = 2\pi/\omega$ the period, and ω the fundamental frequency of the laser field. We use the dipole approximation and the length gauge with the electric-field vector $\mathbf{E}(t) = -d\mathbf{A}(t)/dt$. The rescattering T-matrix element is proportional to (we use atomic units)

$$\int_0^T \frac{dt}{T} e^{iS_{\mathbf{p}}(t)} \int_0^\infty d\tau \left(\frac{2\pi}{i\tau}\right)^{3/2} \langle \mathbf{p}|V(\mathbf{r})|\mathbf{k}_{\rm st}(t,t_0)\rangle \times \langle \mathbf{k}_{\rm st}(t,t_0) + \mathbf{A}(t_0)|\mathbf{r}\cdot\mathbf{E}(t_0)|\psi_{E_i\ell M}\rangle e^{iS_{\mathbf{k}_{\rm st}E_i}(t,t_0)}. \quad (1)$$

The integral is over the rescattering time t and the travel time τ ($t_0 = t - \tau$ is the ionization time), $\mathbf{k}_{\rm st}(t,t_0) = -\frac{1}{t-t_0}\int_{t_0}^t dt' \mathbf{A}(t')$ is the stationary electron momentum, $S_{\mathbf{q}E}(t,t_0) \equiv S_{\mathbf{q}}(t_0) - Et_0 - S_{\mathbf{q}}(t)$, $dS_{\mathbf{q}}(t)/dt = [\mathbf{q} + \mathbf{A}(t)]^2/2$, and $|\mathbf{q}\rangle$ is a plane-wave ket vector such that $\langle \mathbf{r}|\mathbf{q}\rangle = (2\pi)^{-3/2}\exp(i\mathbf{q}\cdot\mathbf{r})$. Notice that as written down this integral extends over positive travel times τ. The matrix elements in (1) are obtained in analytical form, while the double integral is calculated numerically.

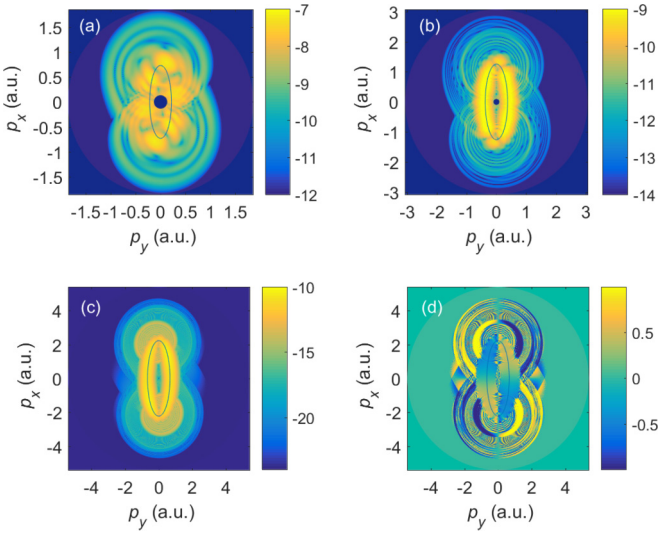

FIG. 1. Logarithm of the differential detachment rate (a)–(c) and the elliptic-dichroism parameter (d) of an F^- ion ($I_p = 3.4$ eV), presented in false colors in the photoelectron momentum plane, for ionization by an elliptically polarized field with $\varepsilon = 0.3$ and intensity 1.3×10^{13} W/cm^2. The wavelength is (a) 1800 nm, (b) 3100 nm, and (c),(d) 5500 nm. The ellipses of the corresponding vector potentials are depicted in each panel. Only the rescattered electrons are included.

We consider the field

$$\mathbf{E}(t) = E_0(\hat{\mathbf{e}}_x \sin\omega t - \hat{\mathbf{e}}_y \varepsilon \cos\omega t)/\sqrt{1+\varepsilon^2}, \quad (2)$$

which is elliptically polarized in the xy plane. The electron is emitted at the angle θ with respect to the x axis so that $\cos\theta = \hat{\mathbf{p}}\cdot\hat{\mathbf{e}}_x$ and $\tan\theta = p_y/p_x$. In Fig. 1 we present the photoelectron momentum distribution for HATI of an F^- ion by a field with the ellipticity $\varepsilon = 0.3$ for three different wavelengths, calculated by numerical evaluation of the double integral (1). We see that the rate satisfies the inversion symmetry $w(\mathbf{p}, \varepsilon) = w(-\mathbf{p}, \varepsilon)$, as it should [38,39]. The high-energy parts of the spectra have the characteristic shape of a slightly distorted and rotated figure eight and a multiplateau structure is visible. It is more pronounced for the longer wavelength of 5500 nm [Fig. 1(c)] where three plateaus are clearly visible, in accordance with the explanation in terms of three dominant pairs of orbits [40], $(\alpha, \beta, m) = \{(\pm1, -1, 0), (\pm1, 1, 1), (\pm1, -1, 1)\}$. However, it is the central part of the spectrum that is most interesting. It changes dramatically with increasing wavelength. For 3100 nm, and even more for 5500 nm, it forms an enhanced region of elliptical shape, which is centered about the vector-potential ellipse $-\mathbf{A}(t)$. For comparison with experimental data or solutions of the time-dependent Schrödinger equation or Monte Carlo trajectory simulations, it must be kept in mind that the direct electrons also contribute to the central part [41].

The symmetry $w(\mathbf{p}, \varepsilon) = w(-\mathbf{p}, \varepsilon)$, i.e., $w(\theta, \varepsilon) = w(\theta + \pi, \varepsilon)$, is valid for the exact ionization rate [38,39]. Symmetry with respect to a change of sign of the ellipticity is also exact: $w(\theta, -\varepsilon) = w(\pi - \theta, \varepsilon) = w(-\theta, \varepsilon)$. The elliptic-dichroism parameter $\delta(\mathbf{p}, \varepsilon) \equiv [w(\mathbf{p}, \varepsilon) - w(\mathbf{p}, -\varepsilon)]/[w(\mathbf{p}, \varepsilon) + w(\mathbf{p}, -\varepsilon)]$, which is zero for the

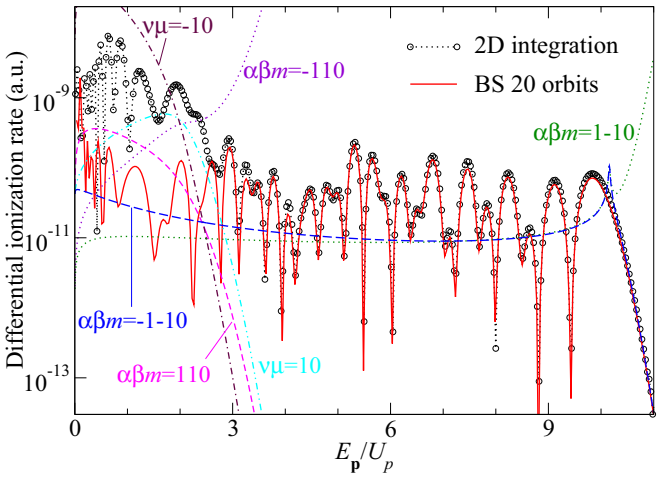

FIG. 2. Differential detachment rate of F^- ions as a function of the photoelectron energy in units of U_p for emission in the direction of the linearly polarized field having the intensity 1.3×10^{13} W/cm^2 and the wavelength 3100 nm. Only the rescattered electrons are included and the results are obtained by numerical integration (black dotted line with circles), by the uniform approximation with 20 backscattering orbits (red solid line), and by using the saddle-point method for particular orbits (α, β, m) and (ν, μ) as indicated.

direct electrons, allows one to assess the contribution of the rescattered electrons to a given final-state momentum $\mathbf{p}$. From Fig. 1(d) we see that $\delta(\mathbf{p}, \varepsilon)$ obeys the twofold symmetry $(\theta \leftrightarrow \theta + \pi)$, and changes its sign for $\theta \to -\theta$ and $\theta \to \pi - \theta$, which is in accordance with the relation $\delta(\mathbf{p}, -\varepsilon) = -\delta(\mathbf{p}, \varepsilon)$. The parameter $\delta(\mathbf{p}, \varepsilon)$ is especially large for momenta where only rescattered electrons contribute. For smaller momenta, around and inside the vector-potential ellipse $-\mathbf{A}(t)$, it is smaller and depends less rapidly on the momentum due to the smoothness of the coffee-bean structure.

The integral (1) can also be calculated using the saddle-point method, which leads to the stationarity conditions that the derivatives of the exponential with respect to the times t_0 and t of the action $S_{\mathbf{p}}(t) + S_{\mathbf{k}_{\rm st}E_i}(t, t_0)$ be equal to zero. These conditions correspond to energy conservation at the times t_0 and t:

$$\tfrac{1}{2}[\mathbf{k}_{\rm st} + \mathbf{A}(t_0)]^2 = E_i, \quad \tfrac{1}{2}[\mathbf{k}_{\rm st} + \mathbf{A}(t)]^2 = \tfrac{1}{2}[\mathbf{p} + \mathbf{A}(t)]^2. \tag{3}$$

The solutions of this system, which depend on the final momentum $\mathbf{p}$, are the complex times t_{0s} and t_s, where, according to the aforementioned classification, the index s is $s \in (\alpha, \beta, m) \cup (\nu, \mu)$ [33,34]. In the saddle-point approximation, we have $T^{\rm res}_{\mathbf{p}E_i\ell M}(n) \approx \sum_s A_s e^{iS_s}$, where A_s and S_s are, respectively, the subintegral factor and the action in (1), calculated at the saddle point s. Which solutions to include into the sum over s and which ones to discard is a central issue of this Letter.

To illustrate the application of the quantum-orbit formalism, in Fig. 2 we present the differential ionization rate for a linearly polarized field and for electron emission in the polarization direction. We see that the result obtained using the uniform approximation with 20 backscattering orbits (α, β, m) (red solid line) is in excellent agreement with the numerically calculated rate (black dotted line with circles) for the plateau and the cutoff region of the spectrum. The cutoff is at $10U_p$ and its position corresponds to the intersection of the contributions of the $(\alpha, \beta, m) = (\pm 1, -1, 0)$ orbits [42]. In the energy region below $3U_p$, the 20 (α, β, m) solutions in the uniform approximation fail to reproduce the numerically calculated spectrum. In this region, the forward-scattered solution $(\nu, \mu) = (1, 0)$ and the solutions $(\alpha, \beta, m) = (\pm 1, 1, 0)$ are dominant.

For a linearly polarized field, it can easily be checked that if (t_{0s}, t_s) is a solution of (3), then $(T - t^*_{0s}, T - t^*_s)$ is another solution with the same imaginary parts of the ionization and rescattering times. In past work, this solution was ignored since the corresponding travel time $\mathrm{Re}\,[T - t^*_s - (T - t^*_{0s})] = \mathrm{Re}\,(t^*_{0s} - t^*_s)$ is negative. As mentioned above, for elliptical polarization the responsible symmetry is violated; hence, if (t_{0s}, t_s) is a solution then, in general, $(T - t^*_{0s}, T - t^*_s)$ is not. However, we expect that a different solution exists, which, for small ellipticity, is close to the former. We denote this solution by an asterisk: $(\alpha, \beta, m)^*$. Now, the rates corresponding to these solutions are different, so that the ellipticity introduces a bifurcation of the rate. We conjecture that the contributions of both the solutions (α, β, m) and $(\alpha, \beta, m)^*$ should be taken into account.

A rigorous justification will be extremely difficult. The corresponding problem is complicated even in the direct-ionization case where there is only one integral over the ionization time, the contour of which has to be rerouted into the complex plane so as to reach (or bypass) the saddle points [43]. In two dimensions, where the integral over the times t_0 and t has to be deformed from the original real half plane ($-\infty < t_0 < t$ and $-\infty < t < \infty$ or $t \in [0, T]$ for a T-periodic field) into four-dimensional complex space, this appears to be prohibitively complicated. There is no reason that would forbid that a saddle point with a travel time having a slightly negative real part and large imaginary part be included as a relevant complex saddle point. In contrast, for real saddle points the extension of the corresponding stationary-phase approximation from one to two dimensions is rather straightforward; see, e.g., Ref. [44].

Let us then support our statement that the bifurcation of the solution (1,1,0) is responsible for the coffee-bean structure in the photoelectron momentum distribution. Figure 3 shows how the contributions of the solutions (1,1,0) and $(1,1,0)^*$ change and diverge from one another with increasing ellipticity. For $\varepsilon = 0$ they are equal, while already for $\varepsilon = 0.1$ the contribution of the solution $(1,1,0)^*$ has become much larger than the one of (1,1,0) by about two orders of magnitude. With the ellipticity further increasing this difference becomes larger still and for $\varepsilon = 0.3$ the (1,1,0) contribution has become negligible, while the contribution of the orbit $(1,1,0)^*$ is dominant and its maximum has shifted to higher energies. Having in mind that the contributions of the other orbits decrease with increasing ellipticity, we conclude that if the ellipticity is larger than some critical value (which is rather low) the contribution of the orbit $(1,1,0)^*$ is dominant. In Fig. 3(d) we show the corresponding saddle-point times t_0 and t. In all cases, $\mathrm{Im}\,t_0 > 0$ so that all these solutions contribute. Moreover, the imaginary parts of the times t_0 and t for the solution (1,1,0)

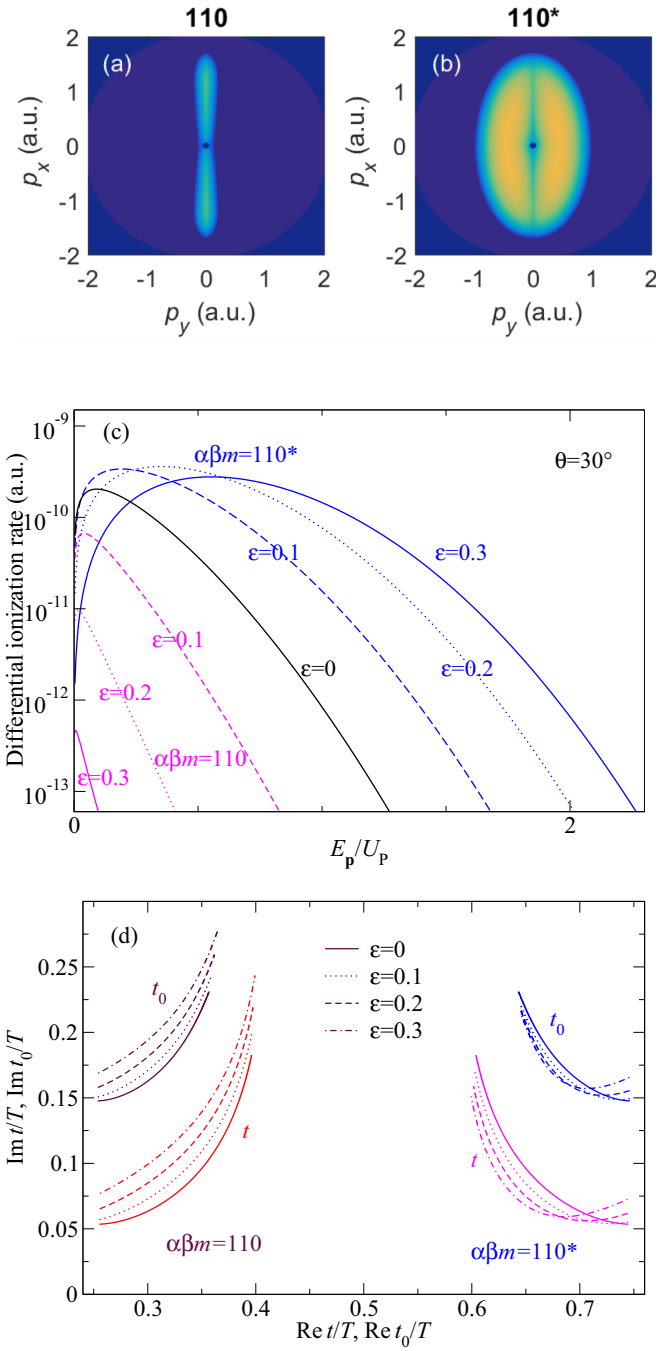

FIG. 3. (a),(b) Logarithm of the differential ionization rate, presented in false colors in the photoelectron momentum plane, for the parameters of Fig. 1 and the wavelength 3100 nm. Only one saddle-point solution [(a) $(\alpha, \beta, m) = (1, 1, 0)$; (b) $(\alpha, \beta, m) = (1, 1, 0)^*$] is taken into account. (c) The differential ionization rate for electron emission in the direction $\theta = 30^\circ$ as a function of the photoelectron energy, for four different values of the ellipticity and the other parameters being the same as in (a),(b). The contributions of the solutions (1,1,0) and (1,1,0)* are presented separately. (d) Saddle-point solutions for the ionization and rescattering times t_0 and t presented in the complex-time plane, for the parameters of (c). The energy $E_\mathbf{p}$ changes from 0 to $5U_p$ along each curve in the direction of larger imaginary parts.

increase with increasing ellipticity so that the corresponding ionization rate decreases. The situation is opposite for the solution (1,1,0)*: the imaginary parts decrease with increasing ellipticity. This explains the dominance of the contribution of the solution (1,1,0)* with increasing ellipticity, as can be seen in the middle panel. Figures 3(a) and 3(b) exhibit the momentum distributions for both solutions. It is clear that the solution (1,1,0)* is responsible for the coffee-bean structure.

Quantum-orbit theory allows for a physical interpretation in terms of complex trajectories that are solutions of the classical Newton equation $\ddot{\mathbf{r}}(t) = -\mathbf{E}(t)$ for an electron in the presence of only the laser field. The quantum process of strong-field ionization starts by tunneling at the complex ionization time t_{0s} and the complex electron trajectory departs from the origin, $\mathbf{r}(t_{0s}) = \mathbf{0}$, with the velocity $\mathbf{k}_{\rm st} + \mathbf{A}(t_{0s})$. At the complex rescattering time t_s, the electron returns to and rescatters off the core at the origin, $\mathbf{r}(t_s) = \mathbf{0}$, whereafter it has the velocity $\mathbf{p} + \mathbf{A}(t_s)$. Quantum orbits are usually defined as complex trajectories as functions of the real time t_R [15]: $\mathbf{r}_{s,-}(t_R) \equiv (t_R - t_{0s})\mathbf{k}_{\rm st} + \int_{t_{0s}}^{t_R} \mathbf{A}(t')dt'$ before rescattering ($\mathrm{Re}\, t_{0s} \leqslant t_R \leqslant \mathrm{Re}\, t_s$) and $\mathbf{r}_{s,+}(t_R) \equiv (t_R - t_s)\mathbf{p} + \int_{t_s}^{t_R} \mathbf{A}(t')dt'$ thereafter ($t_R \geqslant \mathrm{Re}\, t_s$). The corresponding electron trajectories are defined as the real parts of $\mathbf{r}_s(t_R)$. The solutions of the saddle-point equations for the rescattering time t_s usually are approximately real so that, according to the condition $\mathbf{r}_s(t_s) = \mathbf{0}$, the real part of the quantum orbit at the time $t_R = \mathrm{Re}\, t_s$ is approximately equal to zero, i.e., the electron rescatters almost exactly at the origin, $\mathbf{r}_{s,-}(\mathrm{Re}\, t_s) \approx \mathbf{r}_{s,+}(\mathrm{Re}\, t_s) \approx \mathbf{0}$. However, for the orbit (1,1,0)*, due to the large imaginary part of the rescattering time t_s, there is a large discontinuity (jump) in the curve $\mathrm{Re}\, \mathbf{r}_s(t_R)$ at $t_R = \mathrm{Re}\, t_s$, i.e., $\mathrm{Re}\, \mathbf{r}_{s,-}(\mathrm{Re}\, t_s) \neq \mathrm{Re}\, \mathbf{r}_{s,+}(\mathrm{Re}\, t_s)$. So, the classical three-step-model interpretation of the quantum orbits fails. Mathematically, however, the orbit (1,1,0)* is a valid solution of the saddle-point equations. By our conjecture, it must be included and, indeed, it turns out to be necessary to reproduce the exact numerical solution for the HATI spectrum.

To have continuous orbits, complex-time quantum orbits can be introduced, where time proceeds along a path in the complex plane, as has been done in Sec. IV C in [16] and in [30]. We calculate $\mathrm{Re}\, \mathbf{r}_s(t_C)$ for the complex time t_C, which follows the curves

$$\begin{aligned} C_1 &= \{\mathrm{Re}\, t_C = \mathrm{Re}\, t_{0s}, \mathrm{Im}\, t_C \text{ from } \mathrm{Im}\, t_{0s} \text{ to } \mathrm{Im}\, t_s\}, \\ C_2 &= \{\mathrm{Re}\, t_C \text{ from } \mathrm{Re}\, t_{0s} \text{ to } \mathrm{Re}\, t_s, \mathrm{Im}\, t_C = \mathrm{Im}\, t_s\}, \\ C_3 &= \{\mathrm{Re}\, t_C = \mathrm{Re}\, t_s, \mathrm{Im}\, t_C \text{ from } \mathrm{Im}\, t_s \text{ to } 0\}, \\ C_4 &= \{\mathrm{Re}\, t_C > \mathrm{Re}\, t_s, \mathrm{Im}\, t_C = 0\}. \end{aligned} \tag{4}$$

The trajectories along the curves C_1 and C_2 are $\mathrm{Re}\, \mathbf{r}_{s,-}(t_C)$, while along the curves C_3 and C_4 they are $\mathrm{Re}\, \mathbf{r}_{s,+}(t_C)$. The curves are chosen such that the electron trajectory along the union of all curves be continuous and that the aforementioned jump be absent. This is achieved by choosing the curves C_2 and C_3 such that the electron is at the origin at the end of the curve C_2 and at the beginning of the curve C_3, i.e., $\mathbf{r}_{s,-}^{C_2}(t_s) = \mathbf{r}_{s,+}^{C_3}(t_s) = \mathbf{0}$. The electron's path in the complex time plane after departing from the origin at the time t_{0s} is depicted in Fig. 4(a) and the corresponding trajectory in Fig. 4(b). Along each segment C_i, either the real or the imagi-

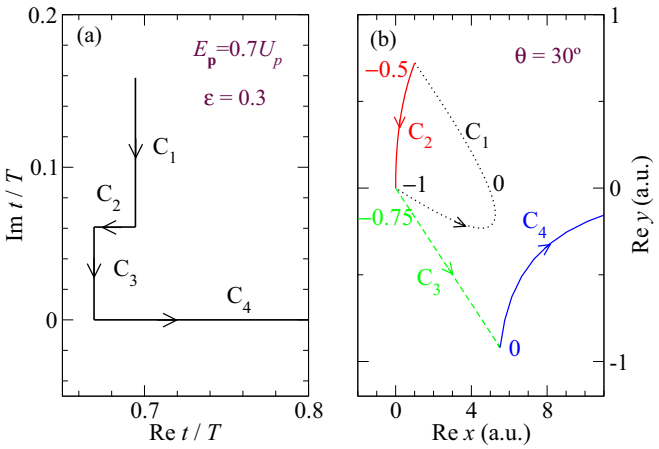

FIG. 4. (a) Complex-time curves defined by (4) for the orbit $(1, 1, 0)^*$. (b) Real part of the orbits for the complex time which follows the curve shown in (a). The field has the ellipticity $\varepsilon = 0.3$, wavelength 3100 nm, and the intensity 1.3×10^{13} W/cm^2. The electron with the energy $E_{\mathbf{p}} = 0.7U_p$ is emitted in the direction $\theta = 30^\circ$. Its energy in units of I_p is also denoted.

nary part of the time is constant, as prescribed by (4). Clearly, along the segment C_2 "time proceeds backwards," while the electron returns to the origin on its way to the act of rescattering. Instead of talking about rescattering, we can say that the "liberated" electron is virtually captured and "bouncing" inside the atomic potential barrier until it is finally "born" at the time $(\mathrm{Re}\, t_s, 0)$. Finally, for real times $\mathrm{Re}\, t_C > \mathrm{Re}\, t_s$, the freed electron moves to the detector along the trajectory that corresponds to the curve C_4. The electron velocity before rescattering is $d\mathbf{r}_{s,-}(t_C)/dt_C = \mathbf{k}_{\mathrm{st}} + \mathbf{A}(t_C)$, while after the rescattering it is $d\mathbf{r}_{s,+}(t_C)/dt_C = \mathbf{p} + \mathbf{A}(t_C)$. The corresponding electron energies are $\mathrm{Re}\,[d\mathbf{r}_{s,\pm}(t_C)/dt_C]^2/2$. The interpretation is the following. The electron starts at the origin with the energy $-I_p$ and moves along the curve C_1 (dotted line). Its energy changes from $-I_p$ to some small positive value and then decreases up to $-0.5I_p$. Then the electron continues along the curve C_2 (solid red line) along which its energy changes from $-0.5I_p$ to $-0.75I_p$. It returns and rescatters off the core at the origin (this corresponds to the under-the-tunneling-barrier recollision [24]). But the imaginary part of the time is still large (contrary to usual rescattering) and we have another virtual motion (dashed green curve C_3). At the start of the curve C_4 the energy is positive, $\mathrm{Im}\, t_C = 0$, and the electron is free.

Concluding, for a laser field with elliptical polarization, we found as legitimate solutions of the saddle-point equations additional quantum orbits with negative travel times and large imaginary parts, which are necessary for a good approximation of the corresponding integral over the ionization and the travel time. These orbits generate a peculiar structure in the velocity map of the rescattered electrons, which is reminiscent of a coffee bean. Since the rescattering matrix element in (1) contains the short-range potential, we expect that the coffee-bean structure (its width and shape) reflects the characteristics of this local potential [45]. We are planning to explore this in our future work. We expect that such structures are even more noticeable in the momentum distribution of the elliptic dichroism parameter [see Fig. 1(d); this parameter is zero for the direct electrons]. If successful, this method can be extended to more complex systems to study, for example, shape resonances in rescattering from molecular targets [49]. It is likely that corresponding orbits also exist for other nonstandard driving fields, such as bicircular fields or orthogonally polarized two-color fields, and may also generate characteristic structures in the velocity map. Our work also shows that whenever the imaginary parts of the saddle-point times that characterize a strong-field process are large, a formalism with complex quantum orbits should be used. In this case the interpretation of the results is not as simple as when the imaginary part of the rescattering time is small, where the process can be well described using classical physics. This may be related to the quantum dynamics with complex classical trajectories, a recently introduced method, which also has been applied to strong-field physics [50].

We acknowledge support by the Ministry of Science, Higher Education and Youth, Canton Sarajevo, Bosnia and Herzegovina, and by the Alexander von Humboldt Foundation.

[1] M. Lewenstein, Ph. Balcou, M. Yu. Ivanov, A. l'Huillier, and P. B. Corkum, Theory of high-harmonic generation by low-frequency laser fields, Phys. Rev. A **49**, 2117 (1994).

[2] M. Lewenstein, K. C. Kulander, K. J. Schafer, and P. H. Bucksbaum, Rings in above-threshold ionization: A quasiclassical analysis, Phys. Rev. A **51**, 1495 (1995).

[3] W. Becker, F. Grasbon, R. Kopold, D. B. Milošević, G. G. Paulus, and H. Walther, Above-threshold ionization: From classical features to quantum effects, Adv. At. Mol. Opt. Phys. **48**, 35 (2002).

[4] D. B. Milošević, Strong-field approximation and quantum orbits, in *Computational Strong-Field Quantum Dynamics: Intense Light-Matter Interactions*, edited by D. Bauer (De Gruyter Textbook, Berlin, 2016), Chap. VII, pp. 199–221.

[5] H. B. van Linden van den Heuvell and H. G. Muller, Limiting cases of excess-photon ionization, in *Multiphoton Processes: Proceedings of ICOMP 4*, Vol. 8 Cambridge Studies in Modern Optics, edited by S. J. Smith and P. L. Knight (Cambridge University Press, London, 1988), pp. 25–34.

[6] P. B. Corkum, Plasma Perspective on Multiphoton Ionization, Phys. Rev. Lett. **71**, 1994 (1993).

[7] P. Salières, B. Carré, L. Le Déroff, F. Grasbon, G. G. Paulus, H. Walther, R. Kopold, W. Becker, D. B. Milošević, A. Sanpera, and M. Lewenstein, Feynman's path-integral approach for intense-laser-atom interactions, Science **292**, 902 (2001).

[8] D. B. Milošević, Phase space path-integral formulation of the above-threshold ionization, J. Math. Phys. **54**, 042101 (2013).

[9] R. Kopold, W. Becker, and M. Kleber, Quantum path analysis of high-order above-threshold ionization, Opt. Commun. **179**, 39 (2000).

[10] M. Bellini, C. Lyngå, A. Tozzi, M. B. Gaarde, T. W. Hänsch, A. L'Huillier, and C. G. Wahlström, Temporal Coherence of

Ultrashort High-Order Harmonic Pulses, Phys. Rev. Lett. **81**, 297 (1998).

[11] P. Salières, A. L'Huillier, P. Antoine, and M. Lewenstein, Study of the spatial and temporal coherence of high-order harmonics, Adv. At. Mol. Opt. Phys. **41**, 83 (1999).

[12] G. G. Paulus, F. Grasbon, H. Walther, R. Kopold, and W. Becker, Channel-closing-induced resonances in the above-threshold ionization plateau, Phys. Rev. A **64**, 021401(R) (2001).

[13] D. B. Milošević and W. Becker, Role of long orbits in high-order harmonic generation, Phys. Rev. A **66**, 063417 (2002).

[14] D. B. Milošević, G. G. Paulus, and W. Becker, Metering the absolute phase of a few-cycle pulse via its high-order above-threshold ionization spectrum, Laser Phys. Lett. **1**, 93 (2004).

[15] D. B. Milošević, G. G. Paulus, D. Bauer, and W. Becker, Above-threshold ionization by few-cycle pulses, J. Phys. B **39**, R203 (2006).

[16] D. B. Milošević, Forward- and backward-scattering quantum orbits in above-threshold ionization, Phys. Rev. A **90**, 063414 (2014).

[17] C. I. Blaga, F. Catoire, P. Colosimo, G. G. Paulus, H. G. Muller, P. Agostini, and L. F. DiMauro, Strong-field photoionization revisited, Nat. Phys. **5**, 335 (2009).

[18] W. Quan, Z. Lin, M. Wu, H. Kang, H. Liu, X. Liu, J. Chen, J. Liu, X. T. He, S. G. Chen, H. Xiong, L. Guo, H. Xu, Y. Fu, Y. Cheng, and Z. Z. Xu, Classical Aspects in Above-Threshold Ionization with a Midinfrared Strong Laser Field, Phys. Rev. Lett. **103**, 093001 (2009).

[19] M. Möller, F. Meyer, A. M. Sayler, G. G. Paulus, M. F. Kling, B. E. Schmidt, W. Becker, and D. B. Milošević, Off-axis low-energy structures in above-threshold ionization, Phys. Rev. A **90**, 023412 (2014).

[20] B. Wolter, C. Lemell, M. Baudisch, M. G. Pullen, X.-M. Tong, M. Hemmer, A. Senftleben, C. D. Schröter, J. Ullrich, R. Moshammer, J. Biegert, and J. Burgdörfer, Formation of very-low-energy states crossing the ionization threshold of argon atoms in strong mid-infrared fields, Phys. Rev. A **90**, 063424 (2014).

[21] B. Wolter, M. G. Pullen, M. Baudisch, M. Sclafani, M. Hemmer, A. Senftleben, C. D. Schröter, J. Ullrich, R. Moshammer, and J. Biegert, Strong-Field Physics with Mid-IR Fields, Phys. Rev. X **5**, 021034 (2015).

[22] W. Becker and D. B. Milošević, Above-threshold ionization for very low electron energy, J. Phys. B **48**, 151001 (2015).

[23] Orbits with very short travel times have been noticed in passing in early papers on high-order harmonic generation. In Ref. [13] they were referred to as "L-orbits" (see Fig. 4 in this reference). They were observed even earlier for HHG by bicircular fields [see Figs. 13 and 14 in D. B. Milošević, W. Becker, and R. Kopold, Generation of circularly polarized high-order harmonics by two-color coplanar field mixing, Phys. Rev. A **61**, 063403 (2000), and several subsequent papers]. For HATI by a linearly polarized field, a fairly extensive discussion was presented in Ref. [16].

[24] M. Klaiber, K. Z. Hatsagortsyan, and C. H. Keitel, Under-the-Tunneling-Barrier Recollisions in Strong-Field Ionization, Phys. Rev. Lett. **120**, 013201 (2018).

[25] D. B. Canário, M. Klaiber, K. Z. Hatsagortsyan, and C. H. Keitel, Role of reflections in the generation of a time delay in strong-field ionization, Phys. Rev. A **104**, 033103 (2021).

[26] D. B. Milošević and F. Ehlotzky, Coulomb and rescattering effects in above-threshold ionization, Phys. Rev. A **58**, 3124 (1998).

[27] Th. Keil, S. V. Popruzhenko, and D. Bauer, Laser-Driven Recollisions under the Coulomb Barrier, Phys. Rev. Lett. **117**, 243003 (2016).

[28] S. V. Popruzhenko, G. G. Paulus, and D. Bauer, Coulomb corrected quantum trajectories in strong-field ionization, Phys. Rev. A **77**, 053409 (2008).

[29] L. Torlina and O. Smirnova, Time-dependent analytical *R*-matrix approach for strong-field dynamics. I. One-electron systems, Phys. Rev. A **86**, 043408 (2012).

[30] E. Pisanty and M. Ivanov, Slalom in complex time: Emergence of low-energy structures in tunnel ionization via complex-time contours, Phys. Rev. A **93**, 043408 (2016).

[31] A. S. Maxwell, A. Al-Jawahiry, T. Das, and C. Figueira de Morisson Faria, Coulomb-corrected quantum interference in above-threshold ionization: Working towards multitrajectory electron holography, Phys. Rev. A **96**, 023420 (2017).

[32] C. Figueira de Morisson Faria and A. S. Maxwell, It is all about phases: Ultrafast holographic photoelectron imaging, Rep. Prog. Phys. **83**, 034401 (2020).

[33] D. B. Milošević, E. Hasović, M. Busuladžić, A. Gazibegović-Busuladžić, and W. Becker, Intensity-dependent enhancements in high-order above-threshold ionization, Phys. Rev. A **76**, 053410 (2007). In the multi-index notation (α, β, m), the index m gives the approximate length of the travel time in multiples of the laser period. For each m there are two pairs of solutions denoted by $\beta = +1$ for the shorter and $\beta = -1$ for the longer travel time. Each of these pairs consists of two orbits with slightly different travel times (distinguished by the index $\alpha = \pm 1$).

[34] W. Becker, S. P. Goreslavski, D. B. Milošević, and G. G. Paulus, Low-energy electron rescattering in laser-induced ionization, J. Phys. B **47**, 204022 (2014). The index $\mu = 0, 1, 2, 3, \ldots$ counts pairs of solutions (the larger the value of μ, the longer the travel time), while the index $\nu = \pm 1$ characterizes the members of each pair (the travel time is shorter for $\nu = -1$ than for $\nu = +1$).

[35] D. B. Milošević and W. Becker, Improved strong-field approximation and quantum-orbit theory: Application to ionization by a bicircular laser field, Phys. Rev. A **93**, 063418 (2016).

[36] B. Fetić, D. B. Milošević, and W. Becker, High-order above-threshold ionisation of atoms and negative ions: channel-closing effects and the low-frequency approximation, J. Mod. Opt. **58**, 1149 (2011). For simplicity we neglect the polarization potential, which can be found included in D. B. Milošević, A. Gazibegović-Busuladžić, and W. Becker, Direct and rescattered electrons in above-threshold detachment from negative ions, Phys. Rev. A **68**, 050702(R) (2003). The more recent references [37] emphasize the importance of the polarization potential in strong-field processes.

[37] N. I. Shvetsov-Shilovski, M. Lein, and L. B. Madsen, Multielectron polarization effects in strong-field ionization: Narrowing of momentum distributions and imprints in interference structures, Phys. Rev. A **98**, 023406 (2018); M. Abu-samha and L. B. Madsen, Effect of multielectron polarization in the strong-field ionization of the oriented CO molecule, *ibid.* **101**, 013433 (2020); A. A. Romanov, A. A. Silaev, M. V. Frolov, and N. V. Vvedenskii, Influence of the polarization of a multielectron

atom in a strong laser field on high-order harmonic generation, **101**, 013435 (2020).

[38] W. Becker, M. Kleber, A. Lohr, G. G. Paulus, H. Walther, and F. Zacher, Electron spectra of above-threshold ionization in elliptically polarized laser fields, Laser Phys. **8**, 56 (1998).

[39] A. Gazibegović-Busuladžić, D. B. Milošević, and W. Becker, High-energy above-threshold detachment from negative ions, Phys. Rev. A **70**, 053403 (2004). The notation is shortened to emphasize the dependence on $\mathbf{p}$ and ε: $w(\mathbf{p},\varepsilon) \equiv w^{\rm res}_{\mathbf{p}E_i\ell M}(n)$.

[40] R. Kopold, D. B. Milošević, and W. Becker, Rescattering Processes for Elliptical Polarization: A Quantum Trajectory Analysis, Phys. Rev. Lett. **84**, 3831 (2000).

[41] M. Li, M.-M. Liu, J.-W. Geng, M. Han, X. Sun, Y. Shao, Y. Deng, C. Wu, L.-Y. Peng, Q. Gong, and Y. Liu, Experimental verification of the nonadiabatic effect in strong-field ionization with elliptical polarization, Phys. Rev. A **95**, 053425 (2017).

[42] The divergent contribution must be neglected after the cutoff; however, in the uniform approximation these two solutions combine to yield the correct result; see C. Figueira de Morisson Faria, H. Schomerus, and W. Becker, High-order above-threshold ionization: The uniform approximation and the effect of the binding potential, Phys. Rev. A **66**, 043413 (2002). The solution $(\nu,\mu) = (-1, 0)$ should be discarded; see [16] for details; the other forward-scattered solutions contribute in the region below $0.1U_p$, which is not of interest here.

[43] A. Jašarević, E. Hasović, R. Kopold, W. Becker, and D. B. Milošević, Application of the saddle-point method to strong-laser-field ionization, J. Phys. A **53**, 125201 (2020).

[44] R. Wong, *Asymptotic Approximations of Integrals* (Academic, Boston, 1989), Chap. VIII.

[45] In the so-called low-frequency approximation [46] the rescattering matrix element $\langle \mathbf{p}+\mathbf{A}(t)|V|\mathbf{k}_{\rm st}+\mathbf{A}(t)\rangle$ is replaced by the exact scattering amplitude $\langle \mathbf{p}+\mathbf{A}(t)|T_V(E_{\mathbf{p}+\mathbf{A}(t)})|\mathbf{k}_{\rm st}+\mathbf{A}(t)\rangle = \langle \psi_{\mathbf{p}+\mathbf{A}(t)}|V|\mathbf{k}_{\rm st}+\mathbf{A}(t)\rangle$. This theory was successful in extracting the information about the differential cross section for electron-atomic ion [47] and electron-molecular ion [48] scattering.

[46] A. Čerkić, E. Hasović, D. B. Milošević, and W. Becker, High-order above-threshold ionization beyond the first-order Born approximation, Phys. Rev. A **79**, 033413 (2009); D. B. Milošević, Low-frequency approximation for above-threshold ionization by a laser pulse: Low-energy forward rescattering, **90**, 063423 (2014).

[47] M. Okunishi, T. Morishita, G. Prümper, K. Shimada, C. D. Lin, S. Watanabe, and K. Ueda, Experimental Retrieval of Target Structure Information from Laser-Induced Rescattered Photoelectron Momentum Distributions, Phys. Rev. Lett. **100**, 143001 (2008); D. Ray, B. Ulrich, I. Bocharova, C. Maharjan, P. Ranitovic, B. Gramkow, M. Magrakvelidze, S. De, I. V. Litvinyuk, A. T. Le, T. Morishita, C. D. Lin, G. G. Paulus, and C. L. Cocke, Large-Angle Electron Diffraction Structure in Laser-Induced Rescattering from Rare Gases, *ibid.* **100**, 143002 (2008).

[48] A. Gazibegović-Busuladžić, E. Hasović, M. Busuladžić, D. B. Milošević, F. Kelkensberg, W. K. Siu, M. J. J. Vrakking, F. Lépine, G. Sansone, M. Nisoli, I. Znakovskaya, and M. F. Kling, Above-threshold ionization of diatomic molecules by few-cycle laser pulses, Phys. Rev. A **84**, 043426 (2011).

[49] F. Brausse, F. Bach, F. Krečinić, M. J. J. Vrakking, and A. Rouzée, Evolution of a Molecular Shape Resonance Along a Stretching Chemical Bond, Phys. Rev. Lett. **125**, 123001 (2020).

[50] W. Koch and D. J. Tannor, A three-step model of high harmonic generation using complex classical trajectories, Ann. Phys. (NY) **427**, 168288 (2021).